Journal of Energy Storage 74 (2023) 109357

Contents lists available at ScienceDirect

Journal of Energy Storage

journal homepage: www.elsevier.com/locate/est

Research papers

Thermal performance of microchannel heat sink integrated with porous medium, slip coefficient and phase change material and machine learning approach

Somayeh Davoodabadi Farahani [a,*], Amirhossien Jazari Mamoei [a], As'ad Alizadeh [b]

[a] School of Mechanical Engineering, Arak University of Technology, 38181-41167 Arak, Iran
[b] Department of Civil Engineering, College of Engineering, Cihan University-Erbil, Erbil, Iraq

ARTICLE INFO

Keywords:
Microchannel heat sink
Non-Newtonian fluid
Porous media
Phase change material
Slip flow
Thermal performance
GMDH

ABSTRACT

In this study, the thermal performance (TP) of the microchannel heat sink (MCHS) under the influence of the slip coefficient on the microchannel wall, the use of porous medium (PM) and phase change material (PCM), and the changes in the geometrical parameters and the shape of the microchannel have been discussed. The flow and energy equations were solved using the finite volume method. The validation of the melting process, slip coefficient, and porous medium with the previous literature demonstrate the high accuracy of the numerical solution, with the difference between the results being <8 %. The results indicate that using a wavy microchannel can improve TP by approximately10.6 % and 5 % compared to smooth and converging microchannels. Additionally, using non-Newtonian fluids with a power characteristic of 0.53 leads to improved TP about 2.8 % by reducing shear stress compared to Newtonian fluids. Furthermore, the presence of slip on the microchannel wall influences the flow pattern, resulting in reduced convection resistance and improved TP about 3.2–3.8 %. The highest TP was observed at a slip coefficient of 0.00001. Incorporating PM in the microchannel (either in the center or around it) can enhance TP by approximately 8–15 % compared to the base state, with greater improvements observed when PM is placed around the microchannel. The type of PM material and the porosity coefficient significantly impact TP. Varying the cross-sectional shape of the microchannel (square, rhombus, and triangle) has a substantial effect on improving TP compared to a circular cross-section, with the highest TP (with a 71 % increase) observed in microchannels with a square cross-section. Lastly, the use of PCM and PM on the active surface leads to a significant TP improvement of over 80 % compared to the base state. Using the Group Method of Data Handling algorithm, thermal resistance was estimated with an R-square value of 0.94 to validate the available data.

1. Introduction

The microchannel heat sink (MCHS) is a highly efficient cooling system used in electronic devices to dissipate heat generated by them. It is a compact and innovative solution designed to handle high heat loads in a limited space. The MCHS consists of multiple microchannels that are carved out of a solid metal block. These channels are incredibly small and offer a large surface area for cooling. The channels are arranged in parallel, and the coolant fluid flows through them in a laminar flow pattern, which enhances heat transfer. The MCHS has many advantages over traditional cooling systems. For instance, it provides a high heat transfer rate, which helps in reducing the size of the heat sink. It also eliminates hotspots and ensures uniform distribution of heat across the heat sink. Another advantage of the MCHS is that it offers low-pressure drop, which means that the coolant fluid can flow at a higher rate without causing any damage to the system. Additionally, this system is highly reliable and requires minimal maintenance, making it a cost-effective solution for electronic devices. The effectiveness of MCHS is highly dependent on several factors, including the geometry of the microchannel, the fluid characteristics, and the surface properties of the heat sink.

Rahmati et al. [1] explored the TP of a non-Newtonian nanofluid consisting of CuO NPS in an offset fin strip MCHS. Their findings demonstrate that an increase in the *Re* enhances the TP by increasing the convective HT coefficient of the working fluid. This outcomes in a favorable reduction in the surface temperature of the CPU and the rate of thermal entropy generation. Miansari et al. [2] inspected the influences

* Corresponding authors.
E-mail address: sdfarahani@arakut.ac.ir (S.D. Farahani).

https://doi.org/10.1016/j.est.2023.109357
Received 5 August 2023; Received in revised form 17 September 2023; Accepted 18 October 2023
Available online 24 October 2023

Nomenclature

D_h	hydraulic diameter(mm)
u_s	Slip velocity(m/s)
C	Specific heat capacity(J/kgK)
f	Fiction factor
n	Power index
Nu	Nusselt number
P	Pressure (Pa)
Po	Poiseuille number
Re	Reynolds number
t	Time(s)
A	Surface(m^2)
B	Slip coefficient
Da	Darcy number
R	Thermal resistance(K/W)
V	Velocity(m/s)
g	Gravity acceleration(m/s^2)
k	Thermal conductivity coefficient(W/mK)
q	Heat flux(W/m^2)

Greek letter

$\dot{\gamma}$	Shear rate(1/s)
ε	Porosity coefficient
Λ	consistency coefficient($Pa.s^n$)
μ	Viscosity (Pa.s)
ρ	Density (kg/m^3)
K	Permeability coefficient(m^2)
Ω	Liquid fraction
β	Thermal expansion coefficient(1/K)
θ	Temperature(K)
τ	Latent heat(J/kg)
φ	Volume fraction

Subscript

f	fluid
in	inlet
s	solid
w	wall

Abbreviation

FVM	finite volume method
GMDH	Group Method of Data Handling Algorithm
HT	Heat transfer
MCHS	Microchannel heat sink
NPS	nanoparticle
PCM	Phase change material
PM	Porous media
TP	Thermal performance

of microchannel height on the HT of the non-Newtonian nanofluid. They observed that an increase in both the channel height and *Re* leads to a decline in temperature, while simultaneously increasing the HT rate and *Nu*. Pahlavannejad et al. [3] inspected the hydrodynamic and thermal behavior of water-CMC- Al_2O_3 in a wavy microchannel with rectangular barriers. Their outcomes displayed that the average *Nu* rises with an intensifying volume fraction of Al_2O_3 NPS. Yao et al. [4] investigated the HT of the water-carboxymethyl cellulose (CMC)/CuO in a silicon MCHS. Ramesh et al. [5] presented Carreau nanodevices through a microchannel with electroosmosis, Joule heating, and chemical reactions. Alnaqi et al. [6] investigated a zigzag MCHS with MWCNTs – SiO_2/EG – H_2O. Their outcomes displayed that growing the speed increases the heat loss from the MCHS. There are other studies on the wave microchannel [7] and the use of nanofluids [8] in improving the HT from the microchannel.

Sarlak et al. [9] considered the numerical optimization of a two-layer MCHS. They showed that the use of carbon-based nanofluid creates a decrease in the *R* of the MCHS compared to metal-oxide nanofluid. Esmailnejad et al. [10] numerically examined the convection HT in a rectangular microchannel. They showed that a significant intensification in the HT of non-Newtonian fluids was observed with the use of NPS, especially in the inlet area. Vasilev et al. [11] directed a computational simulation to compare the performance of seventeen various types of MCHS models with circular pin fins to conventional MCHS. The simulation took into account the effects of diameter, height and distance. Wang et al. [12] studied a MCHS that utilized ribs to chill a chip. In another study [13], it has been shown that the use of PCM and porous medium enhances the TP of MCHS by about 48 %. In similar studies, it was emphasized numerically or experimentally that the use of PCM [12–16] and nano PCM [17] leads to the amendment of the TP of MCHS.

Yousefi et al. [18] optimized the MCHS using the NSGA II algorithm and considering microfluidic effects in the slip flow regime. Jing et al. [19] theoretically studied the efficacy of the slip conditions on the HT of the finned MCHS. They observed that slip conditions can increase the *Nu*. Safikhani et al. [20] conducted a frost creation in micro discontinuous channel heat sinks with the slip velocity. Kumar et al. [21] found that the HT for the slip flow was meaningfully more than for no-slip conditions for a MCHS. Rajalingam et al. [22] analyzed the convective instability of a nanofluid in a vertical porous cylindrical MCHS with the slip conditions. In similar studies [22–24], it was stated that the use of a porous medium is effective on the performance of MCHS. Hung et al. [25] recommended using the conical microchannel to mend the TP of MCHS.

Due to the importance of MCHS, many studies have been done to evaluate its performance. As the literature suggests, extensive research has been conducted to improve the TP of MCHS. To handle fluctuations in heat generated by electronic devices, heat sinks must operate at full capacity, requiring more electric power. While PCM-based passive heat sinks can partially address this issue, they are only effective during the phase-changing process. This study presents a novel PCM-based hybrid MCHS model that combines the advantage of energy storage, providing the ability to manage variable heat generation. According to the authors, no significant research has been done on hybrid MCHS based on PCM, porous material, and non-Newtonian fluid considering the slip condition on microchannel walls so far. This indicates a great potential for advancements in hybrid MCHS for electronic cooling. In the current study, the efficacy of changing the geometric shape of the microchannel (wave, converging, and smooth) with non-Newtonian fluid, and the slip conditions in the microchannel and the presence of PCM on the performance of MCHS has been explored. The influence of *Re*, slip coefficient, and NPS on the TP of the MCHS has been evaluated. The numerical solution based on FVM is employed. A Power-Law non-Newtonian fluid is employed to simulate the viscosity, while the enthalpy-porosity method is utilized to model the melting-freezing process of PCM. The GMDH algorithm is employed to estimate the TP of MCHS.

2. Problem description

Investigating heat transfer inside MCHS requires the simultaneous analysis of conduction HT for the solid and convective HT to the chilling fluid. In this study, the local hot spots created in the heat generator are ignored and the constant heat flux assumption is defined as the thermal boundary condition. For this study, microchannels with a circular cross-section have been used assuming two wall states: no slip and slip.

Straight (C1), wavy(C2) and convergent (C3) MCHS are considered (Fig. 1). The fluid flow is considered incompressible, and laminar. The microchannel with different cross-section (circular, rhombic, triangular, and square) and the distance of the microchannel from the active surface is considered for 7 modes, which is revealed in Fig. 1. Another case has been investigated in which the porous layer partially fills the microchannel (in the center or around the microchannel). Also, the efficacy of the placement of the porous layer& PCM in zone 1 on the TP of MCHS has been inspected. The chilling fluid is water, water-CMC-CuO, and the solid part is made of aluminum. The material of porous media is AL. The characteristics of the materials used are presented in Table 1.The sizes of the computational block are $10 \times 0.7 \times 10\ mm^3$. The inlet temperature is constant at 300 K. The left wall of symmetry and the rest of the revealed walls including the bottom and side walls, are thermal insulation (Figs. 1 and 2).

The fluid flow is considered incompressible, and laminar. The utilization of the Boussinesq approximation has been employed in the modeling of free CHT. Considering the above suppositions, the main equations of the problem will be defined as follows [13,26]:

$$\varepsilon \frac{\partial \rho_f}{\partial t} + \nabla.(\rho_f V) = 0 \tag{1}$$

$$\rho_f \left(\frac{\partial V}{\partial t} + V.\nabla V\right) = -\nabla P + \nabla(\mu_f \nabla V) + Au\frac{(1-\Omega)^2}{(\Omega^3+0.001)}V + \rho_f \beta \varepsilon \vec{g}(\theta-\theta_s) - \left(\frac{\mu_f}{Da.D_h{}^2} + \frac{1.75\rho_f}{\sqrt{150\varepsilon^5 Da.D_h{}^2}}|V|\right)V \tag{2}$$

$$\rho_f \left(C_f + \tau\frac{d\Omega}{d\theta}\right)\frac{d\theta}{dt} + \rho_f C_f V.\nabla\theta = (\varepsilon k_f + (1-\varepsilon)k_s)\nabla^2\theta \tag{3}$$

where $V, \varepsilon, \rho, \mu_f, C, P, Da, k, \tau, \theta, D_h$ and t are velocity, porosity coefficient, density, viscosity, heat capacity, pressure, Darcy number, thermal conductivity coefficient, temperature, hydraulic diameter and time. β is the thermal expansion coefficient. *S&f* are indicated solid and fluid. $Au = 10^5$. The heat equation for the solid medium is considered as follows [13]:

$$k_s \nabla^2 \theta_s = 0 \tag{4}$$

Re, *Da* and Poiseuille number (*Po*) are respectively defined as follows [13]:

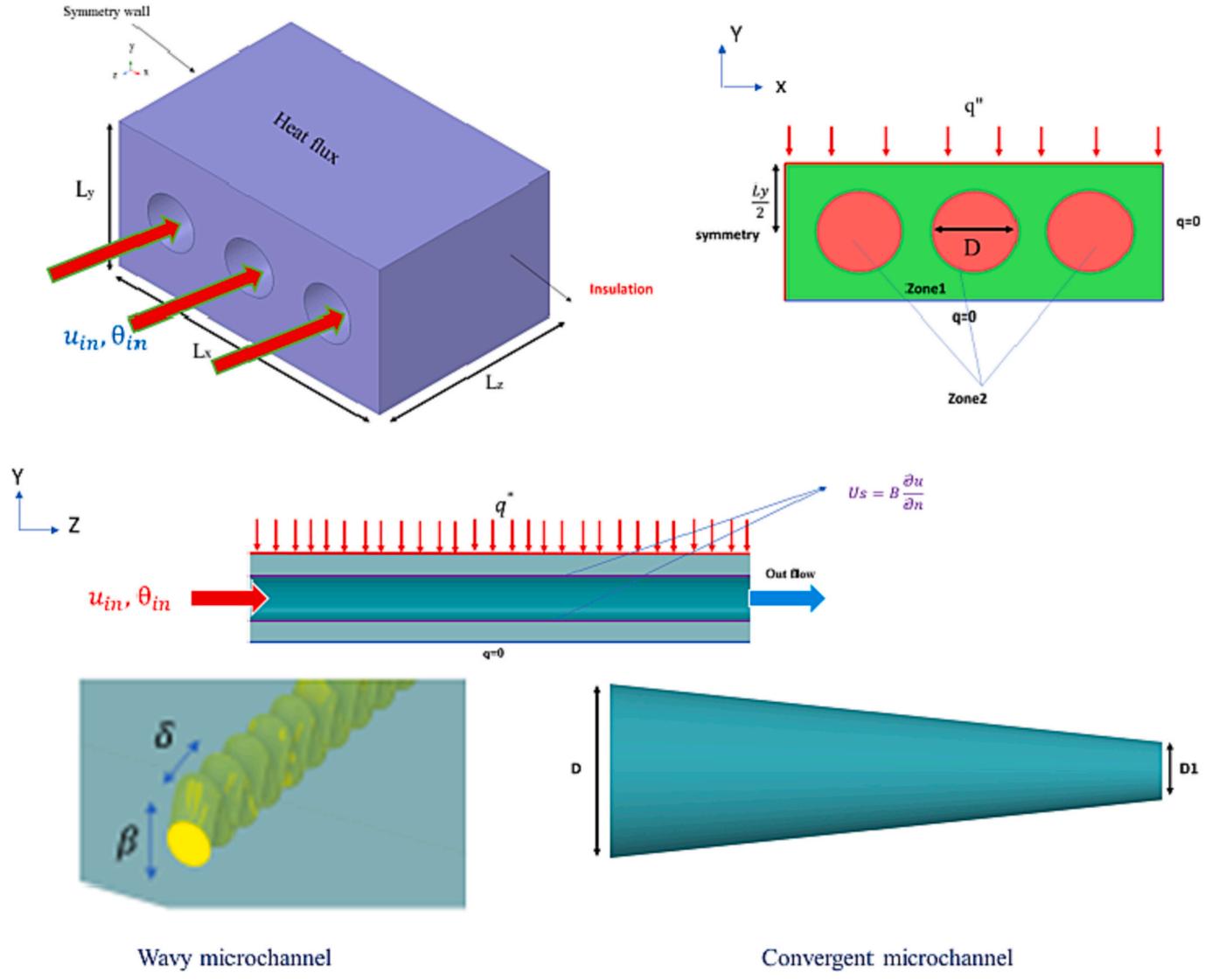

Fig. 1. Geometry and boundary conditions.

Table 1
Characteristics of the materials used in this research [4,28].

Properties	Water	Cuo/water/CMC				AL	Climsel c21 (solid/liquid)
φ(%)	–	0	0.5	1	1.5	–	–
ρ(kg/m^3)	998	1002	1029.49	1056.98	1084.47	2700	1380
C_p(J/kg.K)	4182	4500	4357.97	4223.32	4095.51	871	3600
k(W/m.K)	0.6	0.6	0.602	0.616	0.623	202.4	0.7
β (1/K)	0.000295	–	–	–	–	–	0.0005
μ (Pa.s)	0.001003	–	–	–	–	–	0.01
τ (J/kg)	–	–	–	–	–	–	144,000
Λ (Pa.s^n)	–	0.144	0.144	0.142	0.131	–	–
n	–	0.542	0.541	0.538	0.545	–	–

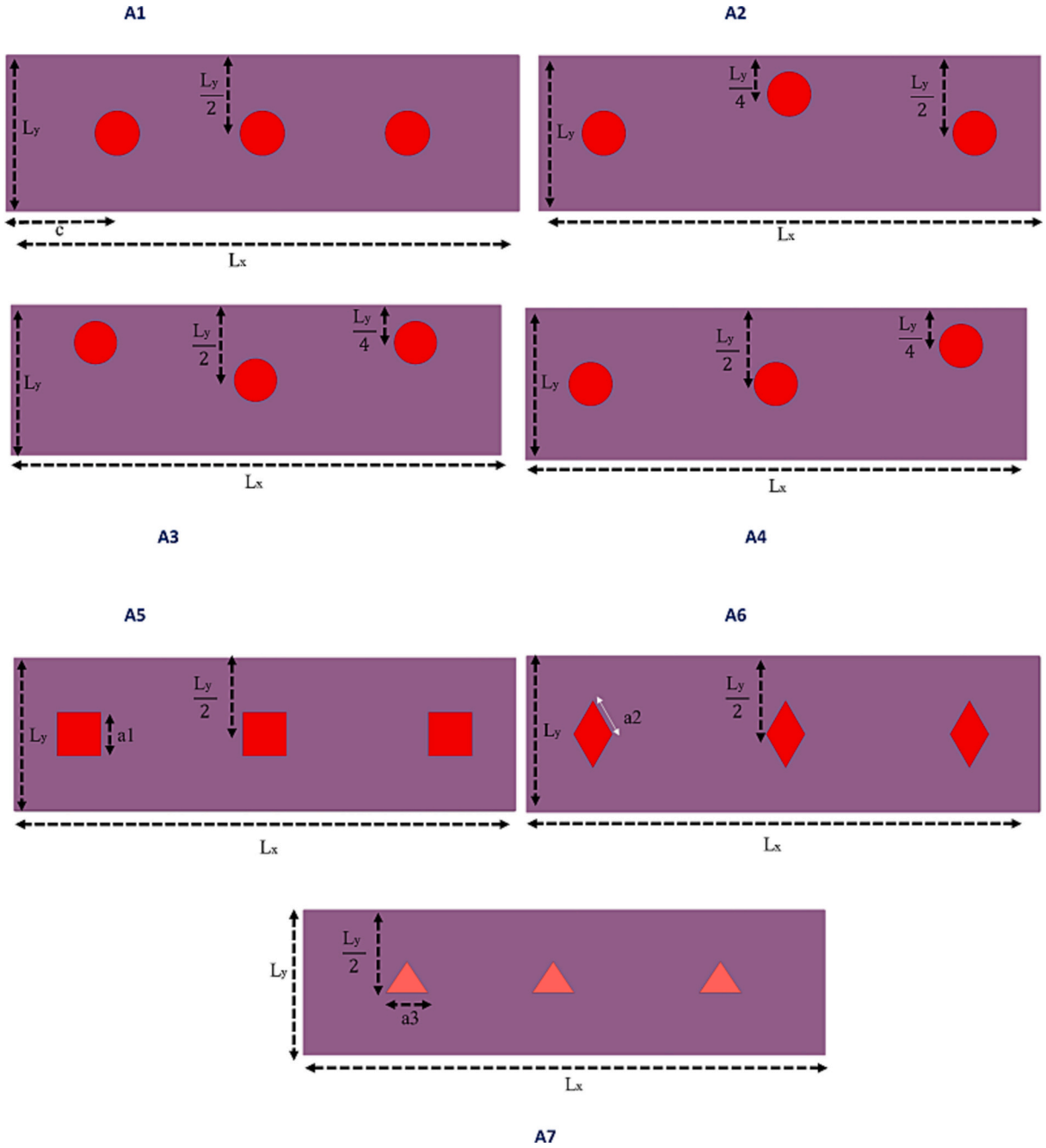

Fig. 2. Considered arrangements of the arrangement of microchannels.

$$Re = \frac{\rho_f V_{inlet} D_h}{u_f} \tag{5}$$

$$Da = \frac{K}{D_h^2} \tag{6}$$

$$Po = \frac{1}{2}\frac{\Delta P}{\rho_f V_{inlet}}\frac{D_h}{L_z} \times Re \tag{7}$$

where V_{inlet} is the inlet velocity. K is the permeability coefficient in the porous material. The thermal resistance of the microchannel (R) is described as follows [11–13,25]:

$$R = \frac{\theta_{w,max} - \theta_{f,inlet}}{qA} \tag{8}$$

where q & A are the heat flux, & area, respectively. The hydrodynamic slip boundary condition is written as follow as [20]:

$$u_s = B\frac{\partial u}{\partial n} \tag{9}$$

B is the slip coefficient and u_s is the slip velocity on the microchannel wall. If the fluid is non-Newtonian, μ_f is defined as follows [27]

$$\mu_f = \Lambda \dot{\gamma}^{n-1} \tag{10}$$

where Λ,n & $\dot{\gamma}$ are the consistency coefficient, power index, and shear rate. ANSYS Fluent software constructed on the FVM was utilized to simulate HT and flow inside the microchannel. According to the Reynolds range of the flow (Re ⟨1000), the laminar flow model is utilized. To investigate conjugate heat transfer, heat transfer is coupled by creating an interface between fluid and solid domains. Boundary conditions are defined in Fig. 1.

To change the boundary conditions on the walls and create slip conditions in Fluent software, the user-defined function (UDF) is typically employed. To apply the slip conditions on the wall, the velocity gradient perpendicular to the surface is calculated and multiplied by the slip coefficient. The SIMPLE algorithm has been utilized to link the V and P fields. Also, spatial discretization for pressure has been considered of second order and for momentum and energy equations, it has been considered in the second-order upwind. Pressure and momentum relaxation coefficients have been taken as 0.25 and 0.65, respectively. To guarantee the convergence of the solutions, the maximum residual value for the Eqs. (1)–(3) has been considered as 10^{-5}, and for the energy equation, it has been considered as 10^{-8}. Most solutions converge after 1200–1600 iterations to the mentioned convergence range. The flowchart of numerical solution was illustrated in Fig. 3a.

To solve the equations on the FVM, it is necessary to convert a physical continuous domain into a computationally discrete domain. That in the areas where the gradients are more severe (such as the areas near the wall), the grid granularity becomes finer. A computing domain is gridded with an organized grid. The quality of the average element is 0.98 and the quality of the lowest element is 0.8. To test the independence of the grid, four grids with the number of meshes:M1(750000), M2(1380000), M3(2275000) and M4(5040000) have been used. The effect of grid dimensions on three parameters influencing the output results (average slip speed and maximum subsurface temperature) has been investigated and shown in Fig. 3b. M4 is considered as the most accurate or basic mode and the amount of error of each mode is for velocity:0.0096,0.0013, and 0.0004 and for temperature: 0.00029,0.00019, &3.2732E-06for M1, M2 and M3, respectively. Due to the lack of significant change in the results between the M3 and M4 modes, the M3 mode meshing is considered the final meshing. This process has been repeated for other geometries to determine the most suitable grid. The selected mesh for two modes C1 and C2 is shown in Fig. 3c. The same process has been repeated for all considered modes to select the appropriate mesh. To confirm the validity of the obtained

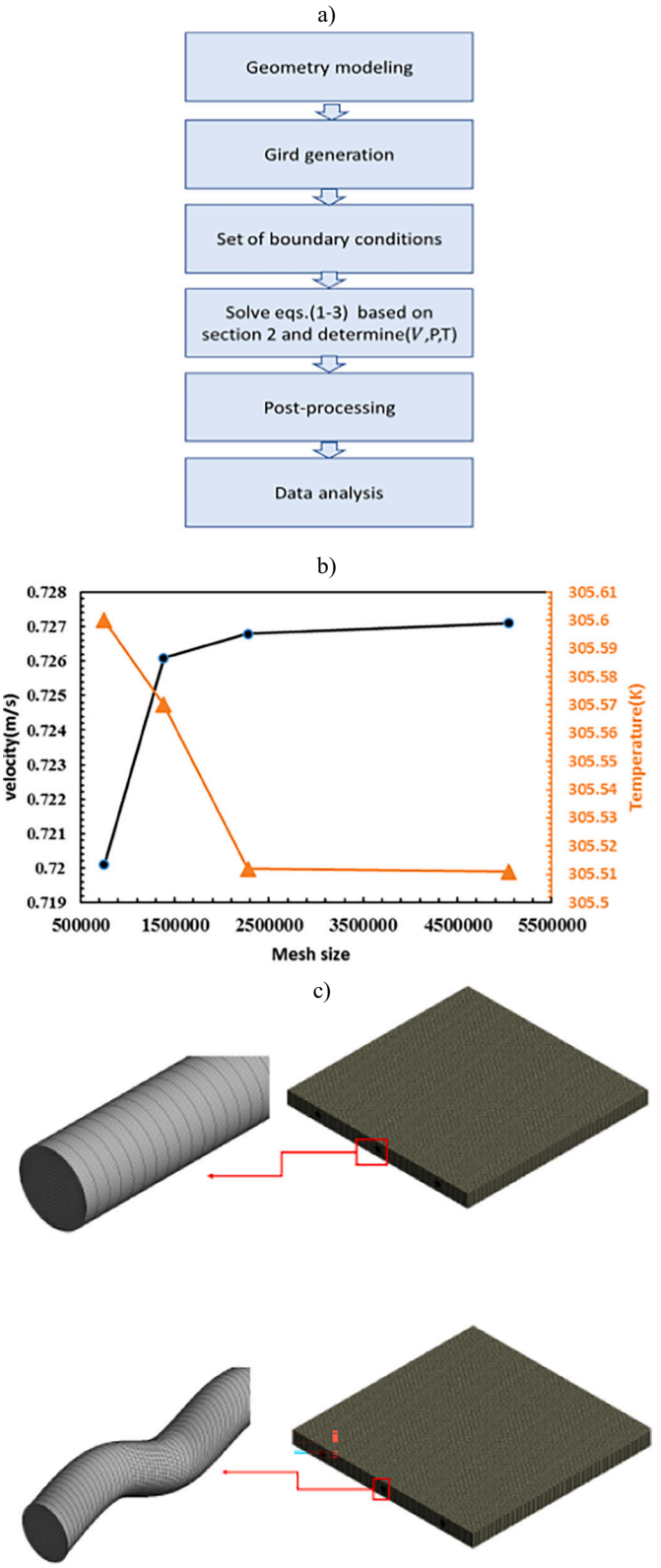

Fig. 3. a) flowchart of numerical solution, b) Grid study for C1 and c)view of selected mesh for C1 and C2.

numerical solutions, the outcomes of the numerical solution should be compared with laboratory results [29]. The mean Nu in the microchannel with D = 0.1 mm is compared with the laboratory study [29] and shown in Fig. 4a. The relative deviation among the results of both analyses is 6.7 %, which indicates the accuracy of the presented

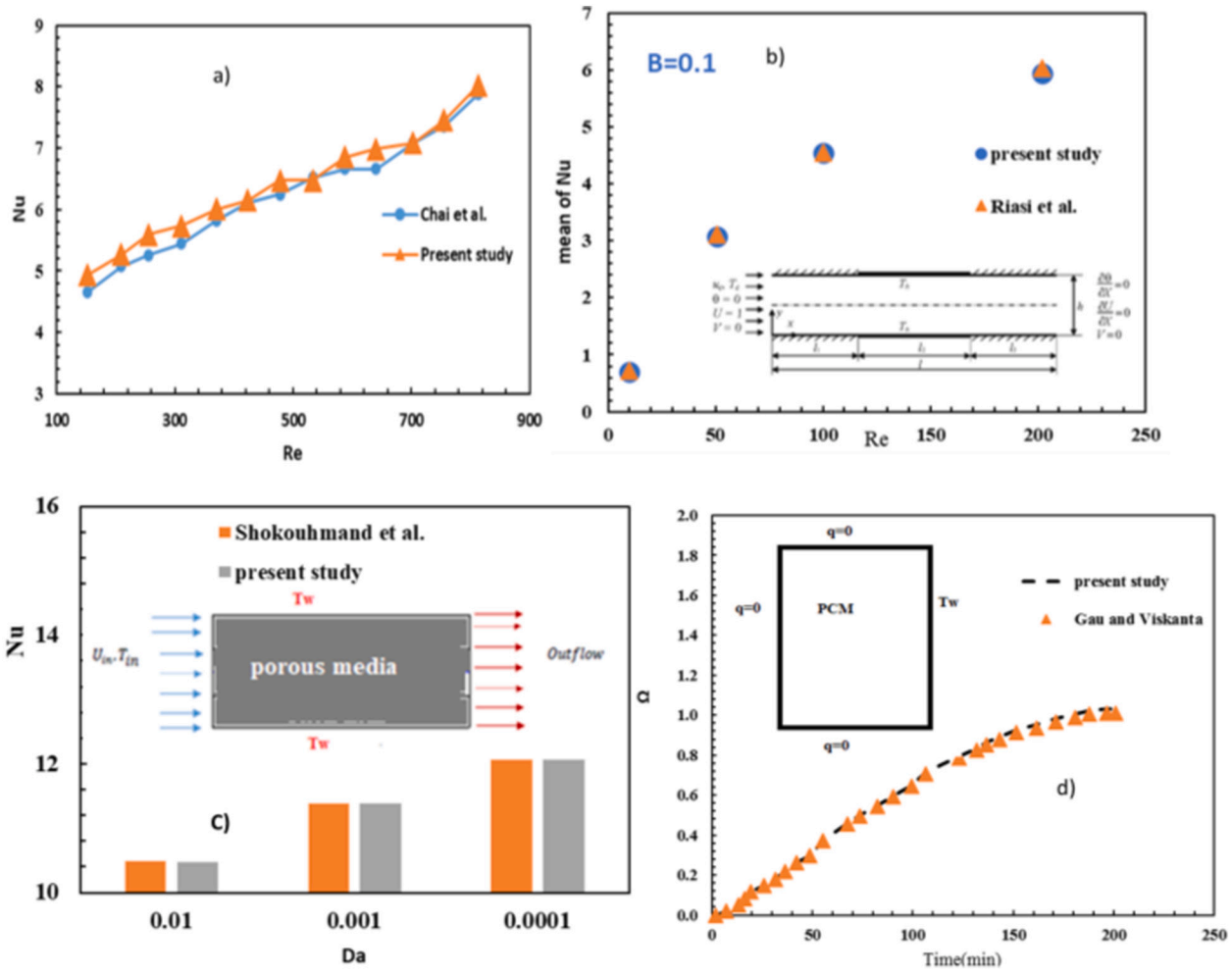

Fig. 4. The validation of the current study with a)Ref. [29],b) Ref. [30],c) Ref. [31], and d) Ref. [32].

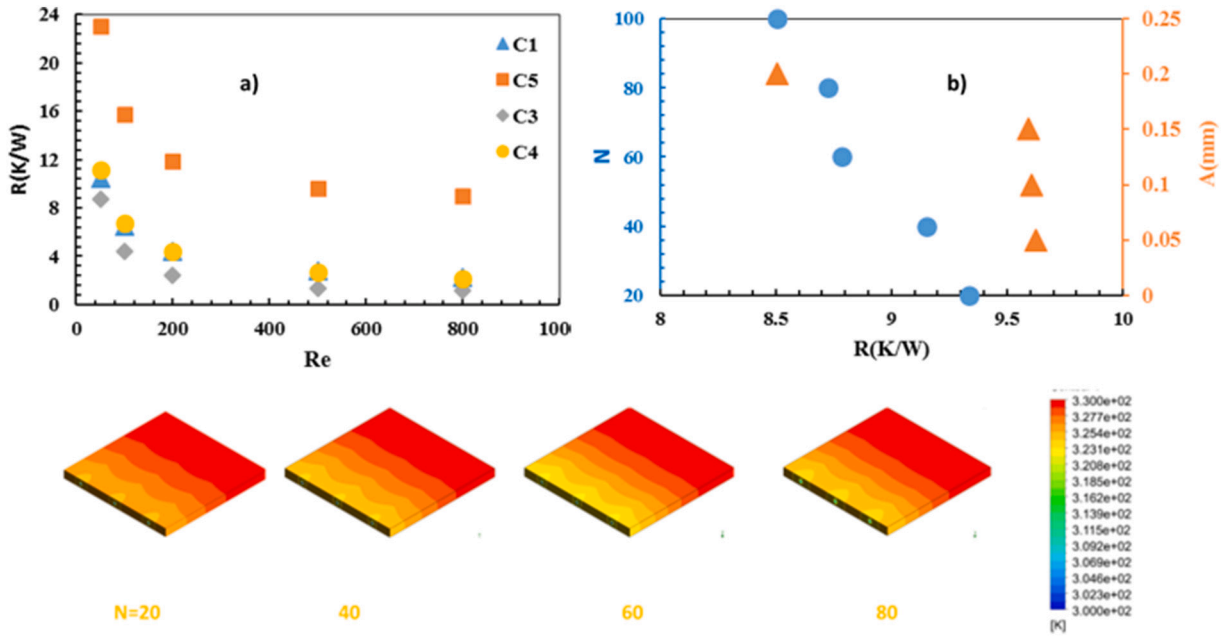

Fig. 5. Effect of a) various geometries and b) geometrical features in C3 on R.

modeling. To validate the average Nusselt number in the present study, it is compared with the results [30] for the microchannel for B = 0.1 at different *Re* and shown in Fig. 4b. The results show a difference of about 4 % and the results are in good agreement with each other. Also, for the porous medium, validation has been done with the results of Shokouhmand et al. [31] for the case where the channel is filled with the porous medium and *Re* = 50, the difference between the results of each study is observed about 7 % (Fig. 4c). To further ensure the correctness and proper performance of the numerical modeling, the history of the melting fraction of the experimental gallium metal melting process by Gau and Viskanta [32] has been modeled and the results are compared in Fig. 4d. As can be seen, the numerical modeling predicts well the location and shape of the melt front and the results differ by <6 %.

3. Results and discussion

Using the presented modeling to examine the TP of MCHS under the impact of changing the geometrical factors and the geometrical shape of the microchannel, non-Newtonian fluid, and slip coefficient on the wall of the microchannel, the use of porous medium and the effect of the characteristics of the medium and the use of PCM have been investigated.

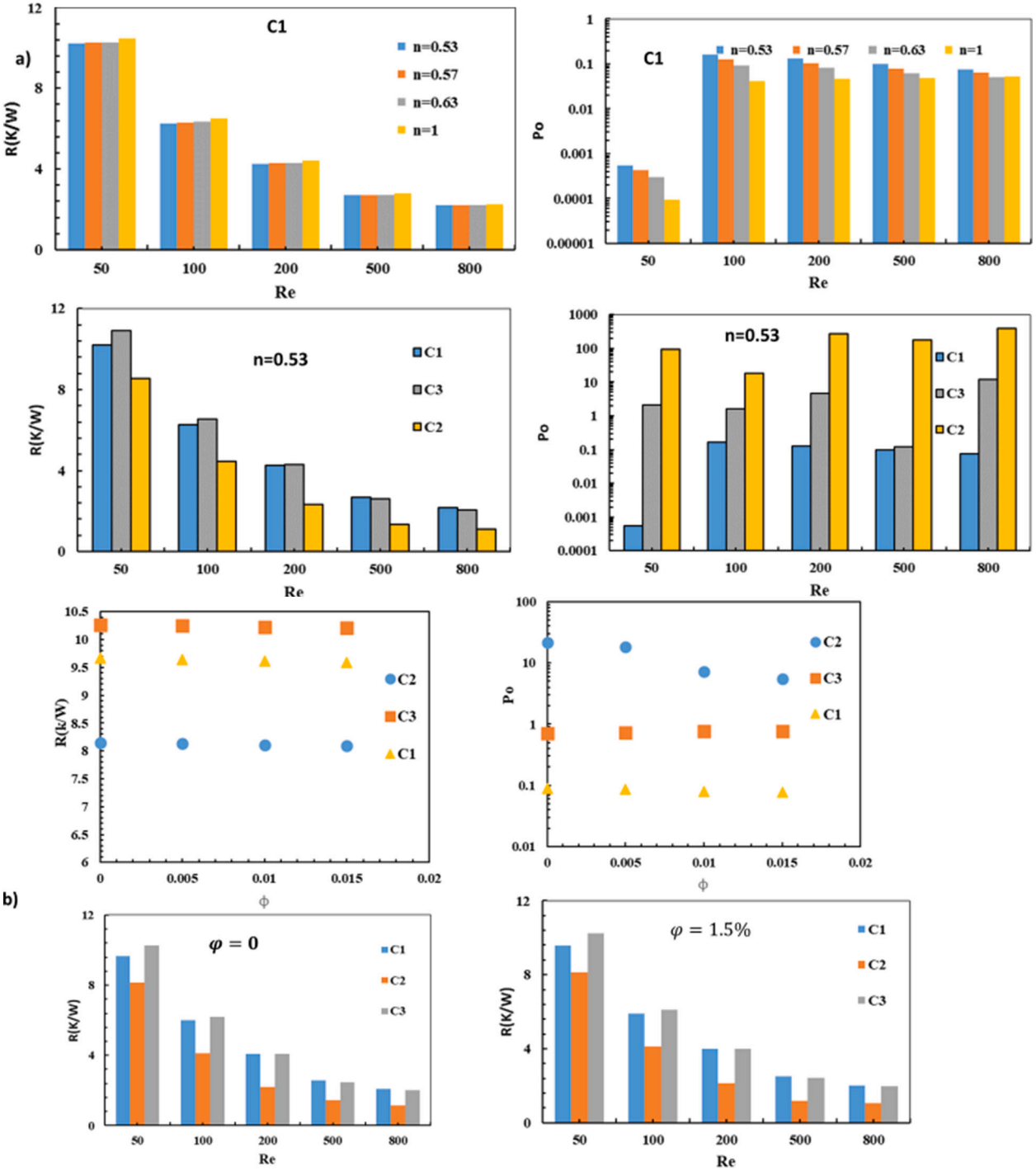

Fig. 6. a)the effect of changing n of Power-law fluid and b) the effect of φ on the TP.

3.1. Analysis of the effective parameters on the TP

In Fig. 5, the effect of changes in frequency and wave amplitude ($\beta\&\delta$) in the wavy microchannel geometry on thermal resistance as well as different geometries for the microchannel has been investigated. With the intensification of *Re*, the *R* decreases in all geometries. The augment in the *Re* means a rise in the flow rate in the microchannel and a diminution in the convection resistance against heat dissipation. Compared to the basic state, the *R* changes for *Re*=50, 100, 200, 500, and 800 for the wavy microchannel are 1.6–5 % and for the convergent state between 3 and 6 % decrease in the thermal resistance has been observed. In the context of a converging microchannel, as the cross-sectional area decreases along the channel, the velocity of flow increases, leading to an increase in the convection heat transfer coefficient. Consequently, the average *R* of convection in the microchannel decreases in comparison to the conventional microchannel state. The wavy microchannel mode has

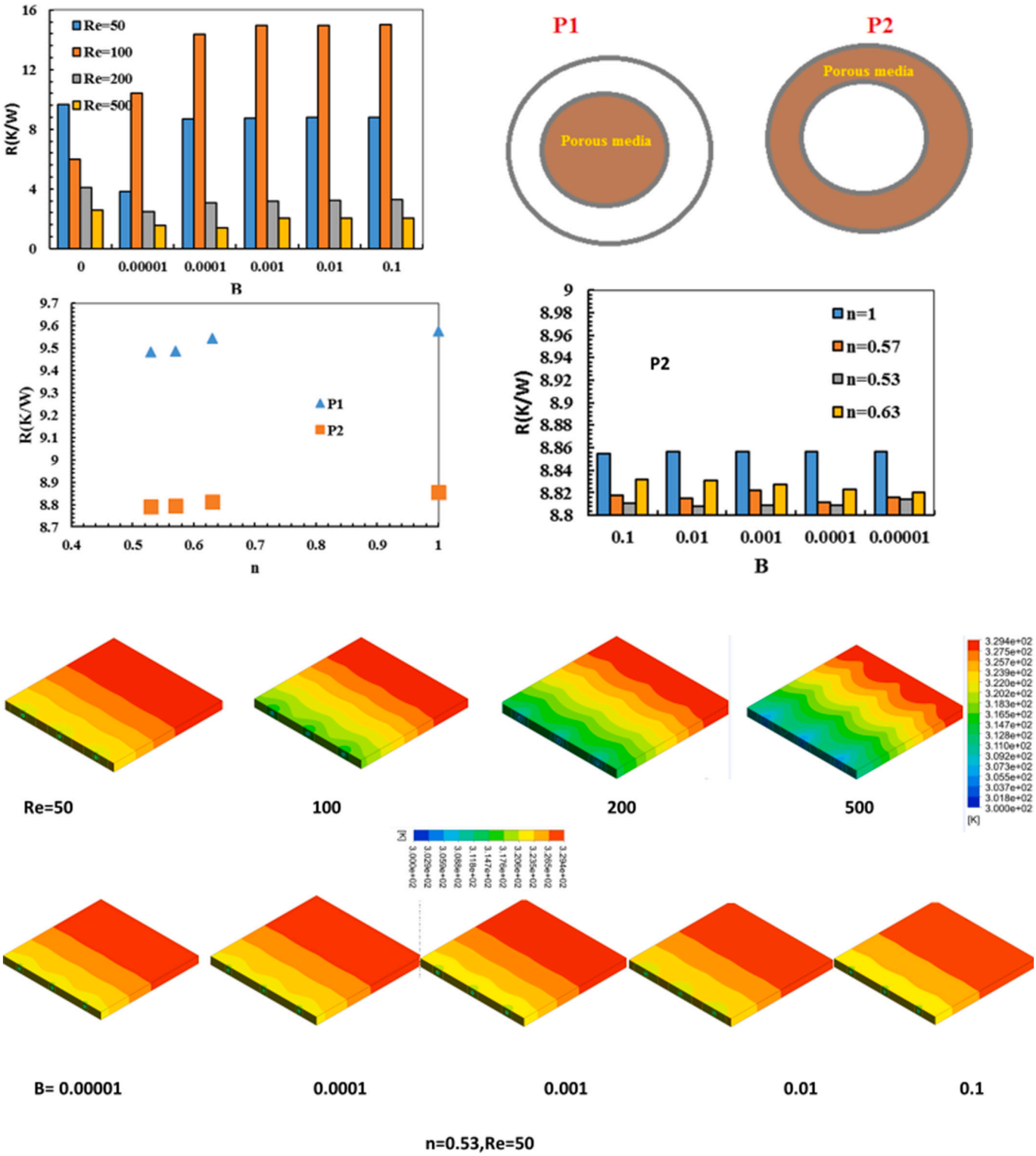

Fig. 7. Effect of slip coefficient and position of the porous medium on the TP of MCHS and temperature contour.

been able to improve the heat dissipation by the microchannel. In addition to creating a temperature gradient along the channel as well as an alteration in the cross-sectional area along the channel, the wavy state of the microchannel wall can augment mixing and the mean temperature in the microchannel, and lead to a reduction in R. With the intensification of δ in the wavy microchannel geometry from 20 to 100 by about 7 % and the phasing of wave amplitude from 0.05 to 0.2 by about 10.6 %, a decrease in thermal resistance of MCHS has been observed. It seems that the increase in the amplitude of the waves due to the changes in the cross-section of the channel and the change in the flow form has a greater effect on the R than the increase in the number of waves along the channel. In the temperature contour, the temperature gradient decreases as the number of δ rises in the heat flux surface.

In Fig. 6, the result of using non-Newtonian fluid on R in different Re and different geometries is investigated. According to the outcomes, with the intensification in the n, the ΔP amplifies, but this increase in ΔP is much more intense at low Re, that is, with the intensification in Re, the effectiveness of the ΔP from changes in the Power-law fluid characteristic decreases. Since the shear stress on the microchannel wall increases with the increase of the n, the velocity gradient in this area will be higher. Also, in a Re, with the increment of n, the capability to dissipate heat from the surface of the heat flux decreases, and with the expansion of the Re, the dependence of heat dissipation on the n decreases. In convective HT, the thermal boundary layer(TBL) thickness is influenced by the viscosity of the fluid. For shear-thinning fluids ($n < 1$), as the shear rate increases, the viscosity decreases, leading to a thinner TBL and enhanced HT. By reducing n from 1 to 0.53 at Re=50, the reduction in R for the wavy microchannel, converging, and tube is approximately 2.1 %, 1.8 %, and 2.3 %, respectively.

The effect of adding CuO NPS to CMC non-Newtonian fluid (0.1 %) on the TP of MCHS in different Re and different φ is shown in Fig. 6. The addition of NPS has increased the k of the base fluid and ultimately increased the HT coefficient, and the R has improved by <0.5 % compared to the state without NPS. One of the interesting points is that the addition of NPS has decreased the power index of the non-Newtonian fluid, and then the ΔPhas decreased with the intensification in the φ of the nanofluid. Of course, this reduction is not significant.

The efficacy of the slip coefficient in MCHS with smooth tube is investigated in several Re and presented in Fig. 7. The slipping of the fluid on the microchannel wall has improved the TP of the MCHS. The lowest value of R has been observed in the B = 0.00001. By increasing B, the slipping speed on the wall can be increased, because the fluid speed in the center of the channel increases. The wall slip can affect the TBL thickness. With the slip flow, the TBL near the walls is thinner, leading to enhanced HT. This is due to the increased mixing and diffusion of heat caused by the altered flow behavior near the walls. Ultimately, this issue will result in improved performance of the MCHS (about 3.2–3.8 %) by reducing the friction drag and increasing the mass flow rate in a fixed and specific pumping power.

The efficacy of the presence of the porous layer in the microchannel on R is shown in Fig. 7. The existence of a partial porous layer within the microchannel enhances the efficiency of heat conduction and alters the thermal resistance of both conduction and convection. By reducing the thermal resistance within the microchannel, it enhances the capability of the microchannel to effectively dissipate heat from the active surface. The presence of the porous layer around the microchannel in the P2 state causes the fluid to be pushed toward the center of the microchannel, and also in the porous region, the coefficient of thermal conductivity increases, following heat transfer, and the thermal resistance helps in heat dissipation. Consequently, the R in the P1 state is greater than in the P2 state. Because the arrangement of the porous medium in the P2 state is caused by strengthening the conduction HT mechanism, it makes an intensification in the HT coefficient in the area near the wall. In state P1, the porous medium is positioned in the middle of the microchannel. The fluid is pushed toward the walls, which can lead to reduced convection resistance and improved HT. Compared to the non-porous state, the enhancement in thermal performance of MCHS is about 7–8.4 % for the P1 state and 13.9–15.3 % for the P2 state. Therefore, the P2 state has a better TP.

In the case of P2, the effect of the slip coefficient on R has been investigated and illustrated in Fig. 7. It can be seen that the R changes slightly by changing n with the increase of B, and this issue is also well observed in the temperature contours. Due to the proximity of the porous medium to the wall, the convection mechanism in this area has a weaker effect than the conduction mechanism. As a result, fluid sliding on the wall in this area is not effective in improving convection flow and cannot be effective in improving TP. By decreasing the n, R decreases and the lowermost value of R is detected at n=0.53. In the following discussion, the efficacy of the characteristics of the porous layer (Darcy number, porosity coefficient, and k_s/k_f) on the TP of MCHS has been inspected and shown in Fig. 8. Changes in the ε from 0.4 to 0.99 have been investigated on the R. By changing the ε from 0.4 to 0.99, the R has increased by about 18.23 %. with the increase of the ε, the value of R has augmented, because with the increase of the ε, the effective k in the porous area decreases and finally the TP of MCHS is weakened. Fig. 8 shows the thermal resistance changes of MCHS for different values of Darcy number. With the increase of Da, the value of Nu has increased and then R has increased. The cause for this behavior is that the rise in Da causes more fluid to flow in the region next to the wall. As can be seen, by increasing the Da from 10^{-6} to 0.1, the R decreases by about 0.01 %. Increasing Da results in an increased fluid penetration into the porous region. This, in turn, can reduce convection resistance and enhance the heat removal capability of the microchannel from the active surface. The changes in the k_s/k_f in the porous region to the convection HT coefficient for the case where the porous layer is placed near the wall and for ε =0.8 and Re= 50 have been investigated and shown in Fig. 7. By intensifying k_s/k_f, the value of the average HT coefficient on the wall has increased in each Darcy number, and by changing this ratio (k_s/k_f) from 0.1 to 10, the heat transfer value has increased by about 83 %. The lowest value of thermal resistance is observed at k_s/k_f=100. Therefore, it can be concluded that the material of the matrix of the porous medium is one of the factors influencing the R. The efficacy of using PCM on the R has been investigated in different conditions and shown in Fig. 8. The PCM is located in a cubic matrix around the microchannels (Zone1). Combined modes with porous medium, the slip coefficient and non-Newtonian fluid have been examined. The outcomes specify that using PCM leads to the improvement of MCHS performance. The PCM material begins to melt by absorbing heat from the active surface. At the beginning of the process, the dominant HT mechanism is conduction, and with the creation of the melted layer, the natural convection HT mechanism is created in the PCM environment. The PCM material has improved the thermal performance by 41 %–90 % compared to the case without PCM. In the case where there is a slip coefficient on the wall, the R is increased by 0.7–2.1 % compared to the non-slip condition. When non-Newtonian fluid with n = 0.53 flows in the microchannel, the R is amended by 0.2–3 % compared to the Newtonian fluid state. When a porous medium is used in the area where PCM is located, an important enhancement in R is observed and this improvement is about 80 %. Since PCM has a low k and at the beginning of the melting process, the HT mechanism is conduction, and the use of a porous medium leads to an enhancement in the effective k and improvement of this mechanism, and ultimately causes heat rejection from the active surface and a decrease in temperature. In this case the value of the melting fraction is higher than in other cases. This issue is well seen in the melting fraction contours.

The effect of PCM location in the microchannel and cross-section on R has been investigated and shown in Fig. 9. The cross-section of the microchannel is circle, square, rhombus, and triangle. The area of the microchannels is equal to each other. The outcomes specify that the shape of the microchannel cross-section has a momentous efficacy on the R, such that the R for microchannels with circular, square, rhombic, and triangular cross-sections is 37 %, 71 %, 24 %, and 51 %,

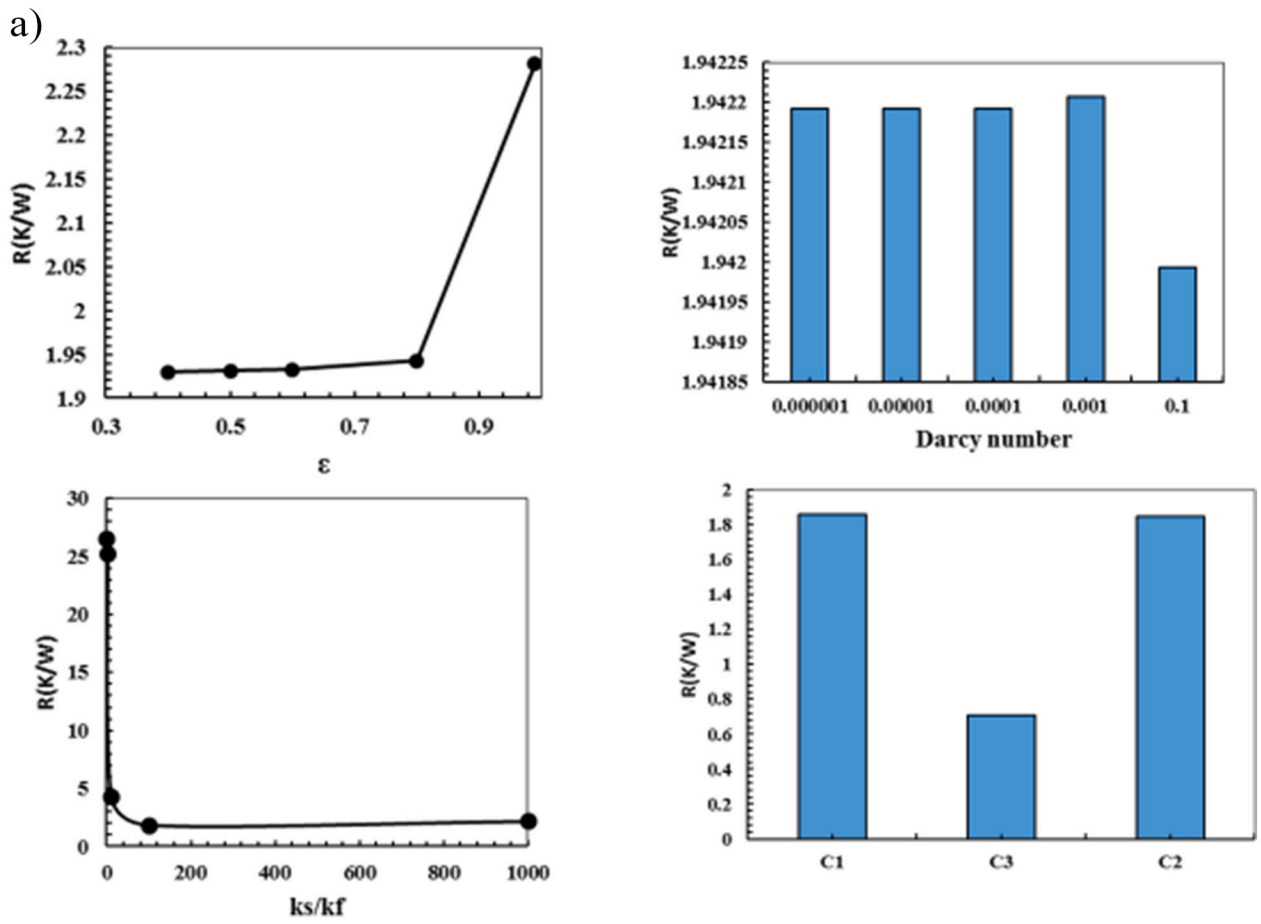

Fig. 8. The effect of the characteristics of a)the porous medium in the P2 state and b) the placement of the porous medium& PCM in zone 1 on the TP of MCH and liquid fraction contour.

respectively, compared to the microchannel mode is improved with a circular cross-section and without PCM. The motivation for this alteration is attributed to the impact of the wall effect. In the scenario of a MCHS with square cross-section, the maximum TP is observed. Also, the effect of the distance of the microchannels from the active surface has been investigated by considering three modes for the arrangement of the microchannels placed in the desired geometry. In the case of A2 and A4, compared to the case of A1, about 7.7 and 3.9 % improvement in thermal performance has been observed. However, the A3 mode could not improve compared to the A1 mode and weakened the performance of MCHS by about 2.1 %. As the microchannel gets closer to the active surface, the thermal resistance in the fluid pathway for heat dissipation decreases, leading to an improvement in TP. At the time of 300 s, the melting fraction contour for the MCHS state with microchannels with different cross-sections is well shown. The results show that in a specific time, the average melting fraction in A1, & A6 modes is at its highest value compared to other modes.

Out of the modes that were investigated, the utilization of PCM and porous media together can enhance thermal efficiency by approximately 80 %. The outcomes of this study's findings can assist electronic component and processor designers and manufacturers in enhancing and optimizing their equipment by exploiting the potential of these examined modes.

3.2. Group method of data handling

Machine learning algorithm and artificial intelligence are the programs that can learn the hidden patterns from the data and predict the output and used for classification or prediction problems [35–38,46]. ANNs are a branch of machine learning algorithms that are built using principles of neuronal organization discovered by connectionism in the biological neural networks constituting animal brains [39–45,47,48]. Group Method of Data Handling (GMDH) is a machine learning algorithm used for modeling and predicting complex systems. It was developed by Ivakhnenko in 1968 and is based on the idea of building a network of polynomial models that adaptively optimize their structure and parameters using a self-organizing approach [33]. The algorithm works by recursively grouping input variables into subsets and fitting polynomial models to each group using a least squares approach. The best model is chosen by using a criterion such as the Akaike Information Criterion or Bayesian Information Criterion. The selected model is then used to predict the output variable [33]. The GMDH theory has resulted in the development of various algorithms, each carefully designed to accommodate specific conditions of a particular application. These algorithms may differ in terms of the elementary function type, the complexity of the model structure, the external criteria, or the modeling task. The selection of the appropriate algorithm is contingent upon factors such as the level of noise present in the data, as well as their adequacy and type. In the early stages, GMDH algorithms made use of probabilistic graphs, Bayes' formulas, and second-order polynomials as elementary functions. Over time, however, the theory has evolved, and GMDH methods have been categorized into two distinct groups: parametric and non-parametric algorithms. Parametric algorithms are recommended for systems with precise or low-variance noisy data, whereas non-parametric algorithms are better suited for systems that are ill-defined and exhibit high-variance noisy data. Parametric algorithms

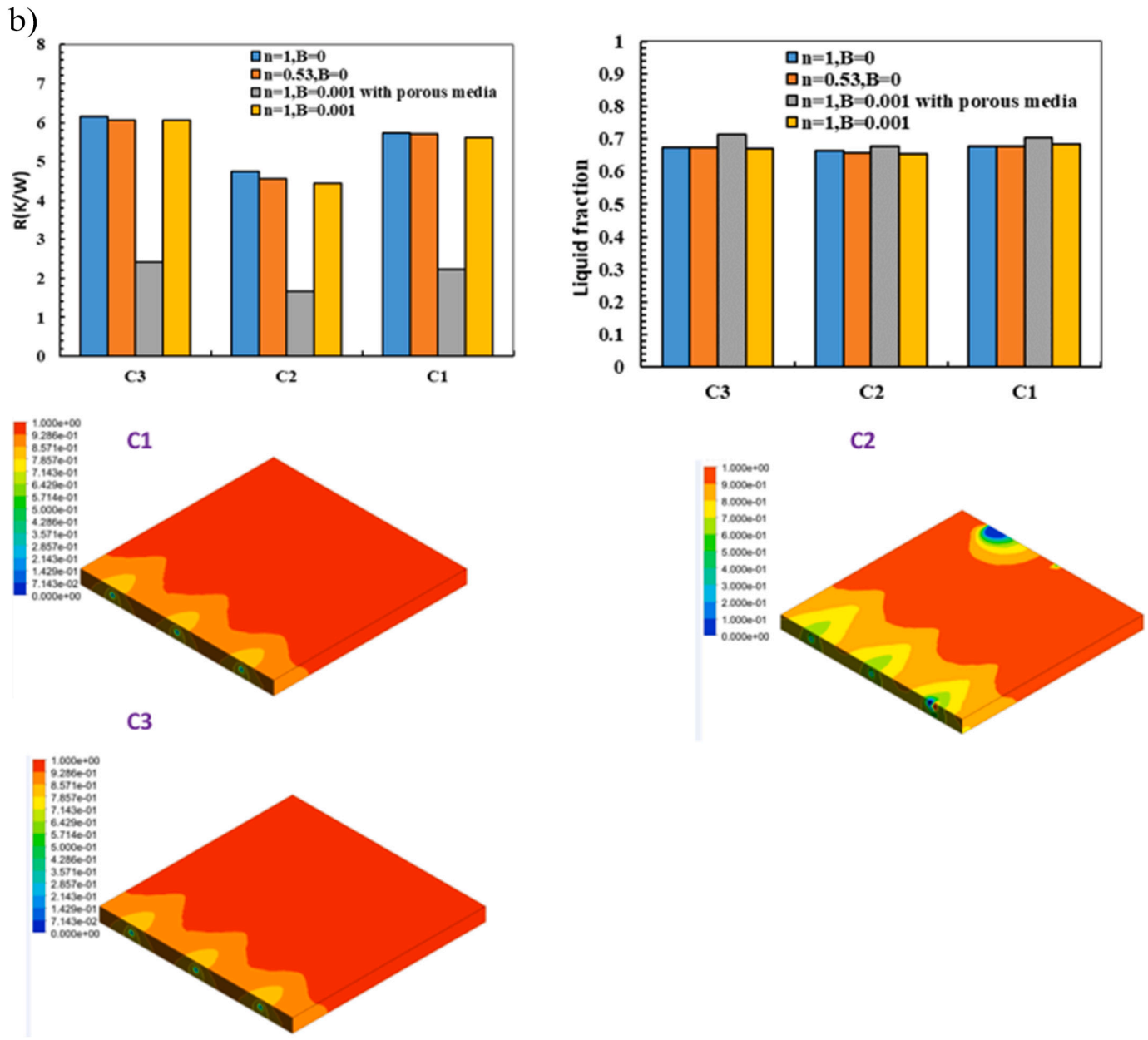

Fig. 8. (*continued*).

can be further classified based on the activation function or the complexity of the model structure. Combinatorial algorithms perform an exhaustive search between all candidate models, while multilayer or iterative algorithms increase model complexity through an iterative procedure. GMDH algorithms can be distinguished based on the type of activation function, including polynomials, harmonic, multiplicative-additive, and fuzzy. The adaptive nature of GMDH algorithms allows for modifications to better suit each application's peculiarities. The GMDH algorithm and structure are well explained in Fig. 10.

The Multilayer GMDH algorithm was initially introduced by Ivakhnenko [33] and has a structure alike to that of multilayer feedforward neural networks as revealed in Fig. 10b. The quantity of layers and nodes is objectively ascertained by an external criterion, in accordance with the incompleteness theorem. The number of nodes in the primary layer corresponds to the number of inputs, while subsequent layers possess nodes equal to the number of pairs of variables for the characteristic vector. The number of hidden units can be preestablished or adjusted based on a threshold value of the external criterion. Multilayer algorithms do not embark on an exhaustive exploration among all potential models; however, if the number of selected models in each layer is sufficiently sizable, the optimal solution will never be forfeited. The second-order polynomial represents the most popular variant of the activation function. Ivakhnenko [34] argues that self-organization is necessary when it becomes impossible to trace all input-output relationships through a complex system. This capability has made GMDH algorithms a suitable modeling procedure for real-world systems. The GMDH algorithm contains four heuristics during the modeling procedure that represent the principal attributes of GMDH theory [34]. Firstly, a collection of observations that appears to be relevant to the object is obtained. Secondly, the observations are categorized into two distinct groups, with the first group utilized for estimating the coefficients of the model, while the second group segregates the information contained within the data into either beneficial or detrimental aspects. Thirdly, a series of elementary functions is generated, whereby the complexity will progressively increase through an iterative process resulting in diverse models. Finally, in accordance with Gödel's incompleteness theorem, an

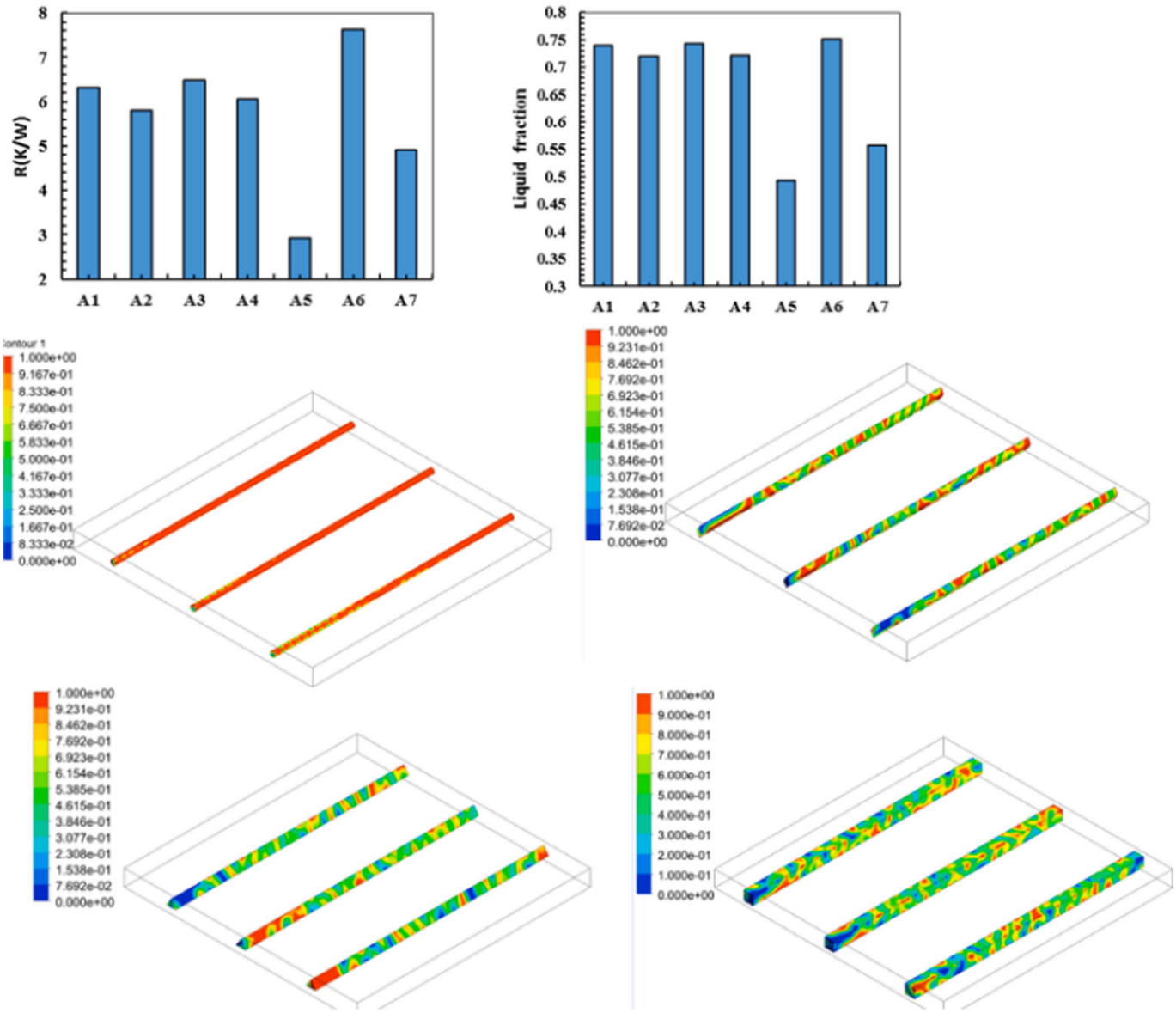

Fig. 9. The effect of the geometric shape of the cross-section and the arrangement of microchannels on the TP and the contour of the melting fraction.

external criterion is employed to select the optimal model.

Input variables for modeling are $\beta, Re, \delta, n, \frac{d}{D}, \varphi, Da,$ *and* ε and output variable is R. Modeling has been done using 108 data. 90 % and 10 % of the data are regarded for training and testing, respectively. The maximum number of neurons in a layer is 15 and the number of layers is 4. The estimation results are presented in Fig. 11. R-square for estimation is 0.94504,0.97006 and 0.94491, for training, test, and all data, respectively. The results show that the GMDH algorithm has been able to estimate R.

4. Conclusion

In the current research, geometric deformation, non-Newtonian fluid (NNF) and slip coefficient on the performance(TP) of MCHS has been investigated. The efficacy of using the porous medium and its characteristics and the use of PCM and its location have been investigated. The equations governing the flow field and temperature were solved using the finite volume method. A Power-Law non-Newtonian fluid is employed to simulate the viscosity, while the enthalpy-porosity method is utilized to model the melting-freezing process of PCM. The GMDH algorithm is employed to estimate the TP of MCHS. The most important findings of this study are:

- By changing the geometric shape of the microchannel from the conventional pipe state to the wavy and converging state, it has been observed that the wavy state exhibits superior performance when compared to other configurations. This modification enhances the TP by approximately 16–50 %. Additionally, the magnitude of the wave amplitude within the microchannel greatly influences the thermal resistance (R).
- Using a Power-law fluid and reducing the power index increases the *Nu* and reduces the convection resistance, resulting in a noticeable 2 % enhancement in the TP. Additionally, applying the slip condition on the microchannel wall reduces the R by 9–19 % in comparison to the non-slip condition.
- Using porous media enhances the effective thermal conductivity coefficient and TP. The percentage increase in TP is dependent on the porosity coefficient, Darcy number, and ratio of solid to liquid conductivity(k_s/k_f). At k_s/k_f=100, the greatest improvement in *TP* has been observed.

a)

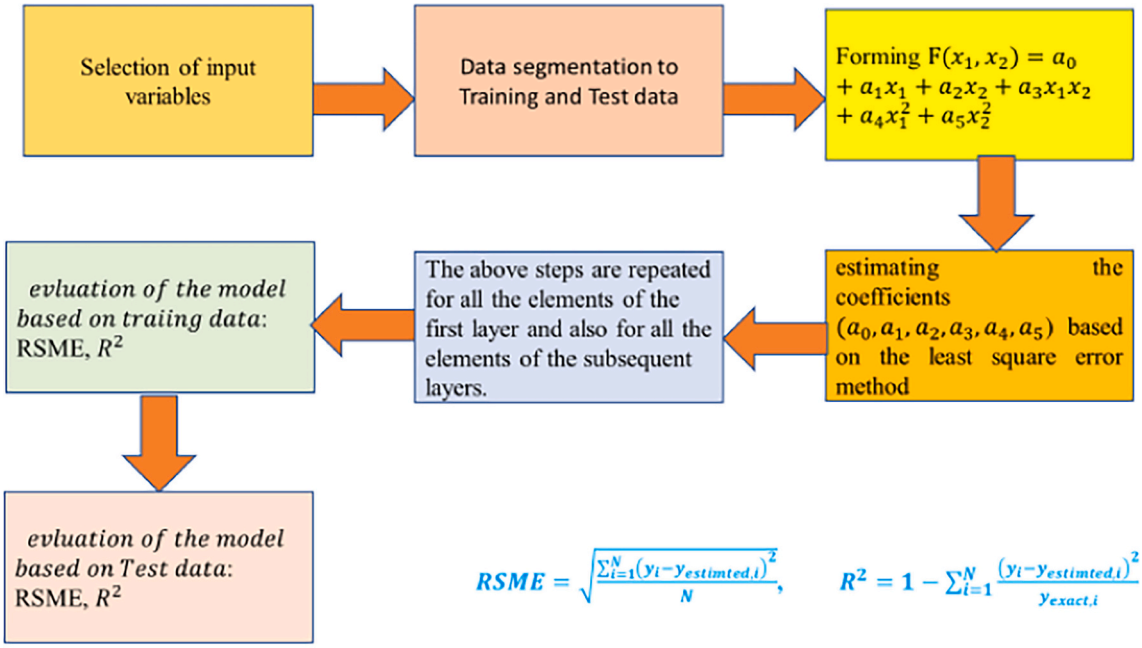

b)

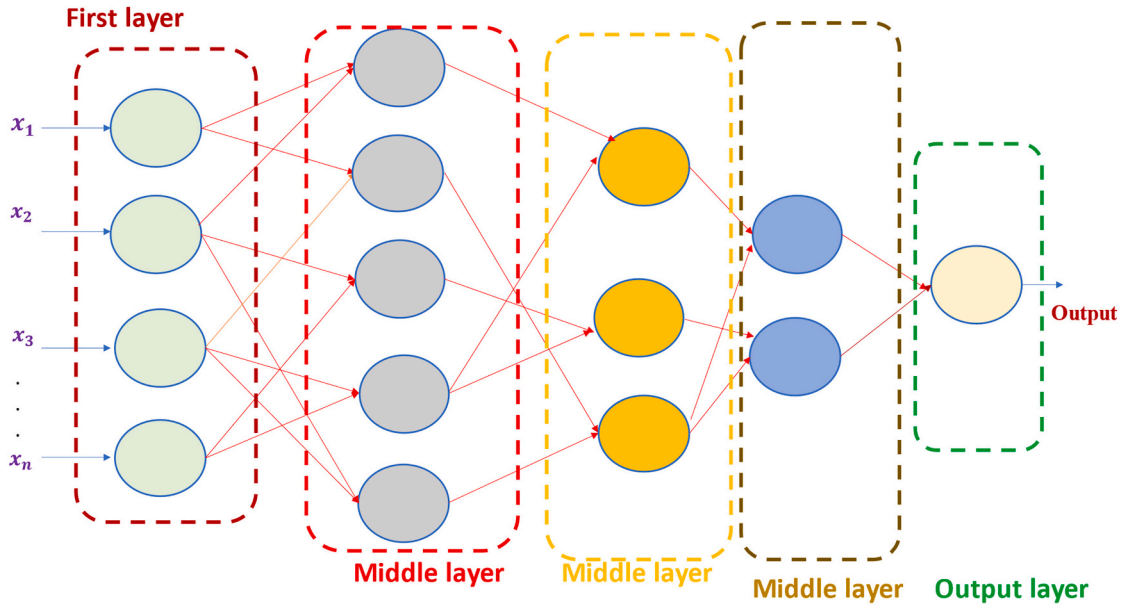

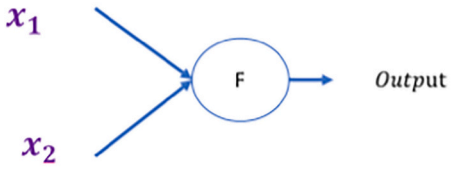

$$Output = F(x_1, x_2) = a_0 + a_1x_1 + a_2x_2 + a_3x_1x_2 + a_4x_1^2 + a_5x_2^2$$

Fig. 10. a) GMDH algorithm, and b) structure of GMDH.

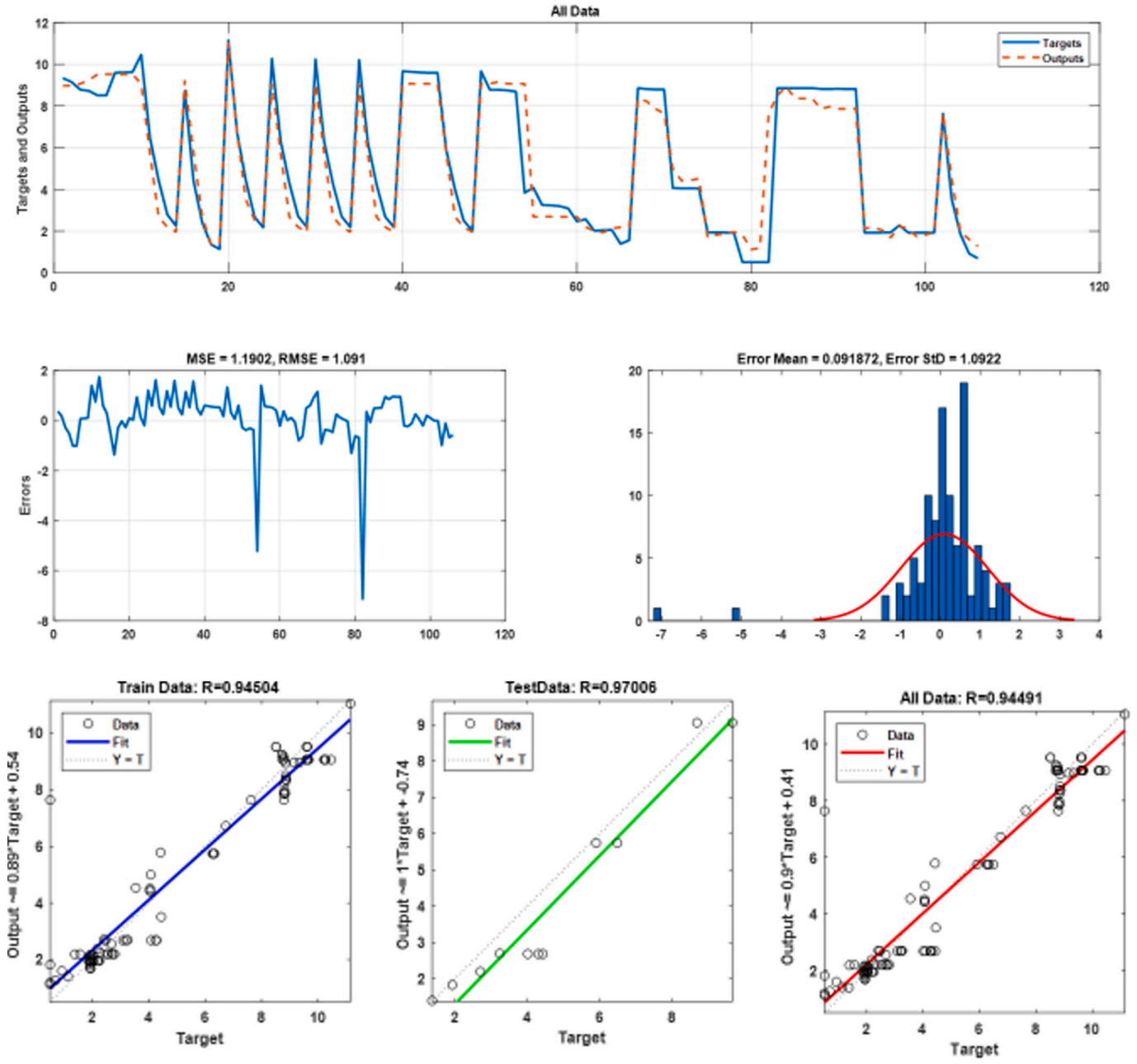

Fig. 11. The estimation of *R* by GMDH.

- The utilization of PCM and porous medium has the potential to enhance the TP by up to 80 %. Additionally, the influence of incorporating PCM in the microchannel and altering its shape (circle, square, rhombus, and triangle) has been examined. It has been observed that the highest TP is achieved when the microchannel has a square cross-section. Nevertheless, regardless of the shape, the TP has been improved with the implementation of PCM compared to the state without PCM.
- Based on the available data and using the GMDH algorithm, *R* was predicted and R-square is 0.94.

Declaration of competing interest

The authors declare that they have no known competing financial interests or personal relationships that could have appeared to influence the work reported in this paper.

Data availability

No data was used for the research described in the article.

References

[1] A.R. Rahmati, M. Derikvand, Numerical study of non-Newtonian nano-fluid in a micro-channel with adding slip velocity and porous blocks, Int. Commun. Heat Mass Transf. 118 (2020), 104843.
[2] M. Miansari, H. Aghajani, M. Zarringhalam, D. Toghraie, Numerical study on the effects of geometrical parameters and Reynolds number on the heat transfer behavior of carboxy-methyl cellulose/CuO non-Newtonian nanofluid inside a rectangular microchannel, J. Therm. Anal. Calorim. 144 (2021) 179–187.
[3] N. Pahlevaninejad, M. Rahimi, M. Gorzin, Thermal and hydrodynamic analysis of non-Newtonian nanofluid in wavy microchannel, J. Therm. Anal. Calorim. 143 (2021) 811–825.
[4] Z. Yao, M. Derikvand, M.S. Solari, J. Zhang, F.M. Altalbawy, A.H.D. Al-Khafaji, O. A. Akbari, D. Toghraie, I.M. Mohammed, Numerical assessment of the impacts of non-Newtonian nanofluid and hydrophobic surfaces on conjugate heat transfer and

irreversibility in a silicon microchannel heat-sink, J. Taiwan Inst. Chem. Eng. 142 (2023), 104642.
[5] K. Ramesh, F. Mebarek-Oudina, A. Ismail, B. Jaiswal, A. Warke, R. Lodhi, T. Sharma, Computational analysis on radiative non-Newtonian Carreau nanofluid flow in a microchannel under the magnetic properties, Sci. Iran. 30 (2) (2023) 376–390.
[6] A.A. Alnaqi, J. Alsarraf, A.A. Al-Rashed, M. Afrand, Thermal-hydraulic analysis and irreversibility of the MWCNTs-SiO2/EG-H2O non-Newtonian hybrid nanofluids inside a zigzag micro-channels heat sink, Int. Commun. Heat Mass Transf. 122 (2021), 105158.
[7] A. Anvari, K. Javaherdeh, Thermal performance of a mini-channel heat exchanger (MCHE) working with CNT/GNP-based non-Newtonian nanofluids, J. Therm. Anal. Calorim. 145 (5) (2021) 2307–2319.
[8] W. Ajeeb, M.S. Oliveira, N. Martins, S.S. Murshed, Forced convection heat transfer of non-Newtonian MWCNTs nanofluids in microchannels under laminar flow, Int. Commun. Heat Mass Transf. 127 (2021), 105495.
[9] A. Sarlak, A. Ahmadpour, M. Hajmohammadi, Thermal design improvement of a double-layered microchannel heat sink by using multi-walled carbon nanotube (MWCNT) nanofluids with non-Newtonian viscosity, Appl. Therm. Eng. 147 (2019) 205–215.
[10] A. Esmaeilnejad, H. Aminfar, M.S. Neistanak, Numerical investigation of forced convection heat transfer through microchannels with non-Newtonian nanofluids, Int. J. Therm. Sci. 75 (2014) 76–86.
[11] M. Vasilev, R.S. Abiev, R. Kumar, Effect of circular pin-fins geometry and their arrangement on heat transfer performance for laminar flow in microchannel heat sink, Int. J. Therm. Sci. 170 (2021), 107177.
[12] H. Zhu, Y. Lu, L. Cai, Wavelength-shift-free racetrack resonator hybrided with phase change material for photonic in-memory computing, Optics Express 31 (12) (2023) 18840–18850, https://doi.org/10.1364/OE.489525.
[13] S.D. Farahani, A.D. Farahani, E. Hajian, Effect of PCM and porous media/nanofluid on the thermal efficiency of microchannel heat sinks, Int. Commun. Heat Mass Transf. 127 (2021), 105546.
[14] L. Lin, Y.-Y. Chen, X.-X. Zhang, X.-D. Wang, Optimization of geometry and flow rate distribution for double-layer microchannel heat sink, Int. J. Therm. Sci. 78 (2014) 158–168.
[15] N. Patel, H.B. Mehta, Experimental investigations on a variable channel width double layered minichannel heat sink, Int. J. Heat Mass Transf. 165 (2021), 120633.
[16] C. Ho, S.-T. Hsu, S. Rashidi, W.-M. Yan, Water-based nano-PCM emulsion flow and heat transfer in divergent mini-channel heat sink—an experimental investigation, Int. J. Heat Mass Transf. 148 (2020), 119086.
[17] C. Ho, S.-T. Hsu, J.-H. Jang, S.F. Hosseini, W.-M. Yan, Experimental study on thermal performance of water-based nano-PCM emulsion flow in multichannel heat sinks with parallel and divergent rectangular mini-channels, Int. J. Heat Mass Transf. 146 (2020), 118861.
[18] M. Yousefi, H. Safikhani, H. Shabani, Multi-objective Pareto Optimization of Frost Formation in Interrupted Micro Channel Heat Sinks (MCHS) Considering Microfluidic Effects in Slip Regime.
[19] D. Jing, J. Song, Y. Sui, Hydraulic and thermal performances of laminar flow in fractal treelike branching microchannel network with wall velocity slip, Fractals 28 (02) (2020) 2050022.
[20] H. Safikhani, H. Shaabani, Numerical simulation of frost formation in interrupted micro channel heat sinks considering microfluidic effects in slip regime, Int. J. Eng. 33 (12) (2020) 2556–2562.
[21] R. Kumar, Physical effects of variable fluid properties on gaseous slip-flow through a micro-channel heat sink, J. Therm. Eng. 7 (3) (2021) 635–649.
[22] A. Rajalingam, S. Chakraborty, Effect of shape and arrangement of micro-structures in a microchannel heat sink on the thermo-hydraulic performance, Appl. Therm. Eng. 190 (2021), 116755.
[23] H. Xu, Thermal transport in microchannels partially filled with micro-porous media involving flow inertia, flow/thermal slips, thermal non-equilibrium and thermal asymmetry, Int. Commun. Heat Mass Transf. 110 (2020), 104404.
[24] R. Chein, J. Chen, Numerical study of the inlet/outlet arrangement effect on microchannel heat sink performance, Int. J. Therm. Sci. 48 (8) (2009) 1627–1638.
[25] T.-C. Hung, W.-M. Yan, Effects of tapered-channel design on thermal performance of microchannel heat sink, Int. Commun. Heat Mass Transf. 39 (9) (2012) 1342–1347.
[26] S.D. Farahani, A.D. Farahani, A.J. Mamoei, H.F. Öztop, Scrutiny of melting rate of phase change material in a four petals cavity with internal branch fins under magnetic field, J. Magn. Magn. Mater. 575 (2023), 170727.
[27] S.D. Farahani, M. Hosseni, A. Zakinia, H.F. Öztop, Control of non-Newtonian fluid flow and heat transfer in microchannel by using porous triangular ribs and pulsating jet, Eur. Phys. J. Plus 137 (6) (2022) 737.
[28] K. Feng, H. Zhang, Pressure drop and flow pattern of gas-non-Newtonian fluid two-phase flow in a square microchannel, Chem. Eng. Res. Des. 173 (2021) 158–169.
[29] L. Chai, G. Xia, L. Wang, M. Zhou, Z. Cui, Heat transfer enhancement in microchannel heat sinks with periodic expansion–constriction cross-sections, Int. J. Heat Mass Transf. 62 (2013) 741–751.
[30] A. Raisi, B. Ghasemi, S. Aminossadati, A numerical study on the forced convection of laminar nanofluid in a microchannel with both slip and no-slip conditions, Numer. Heat Transf. A Appl. 59 (2) (2011) 114–129.
[31] H. Shokouhmand, F. Jam, M. Salimpour, The effect of porous insert position on the enhanced heat transfer in partially filled channels, Int. Commun. Heat Mass Transf. 38 (8) (2011) 1162–1167.
[32] C. Gau, R. Viskanta, Melting and Solidification of a Pure Metal on a Vertical Wall, 1986.
[33] S.J. Farlow, The GMDH algorithm of Ivakhnenko, Am. Stat. 35 (4) (1981) 210–215.
[34] A. Ivakhnenko, Heuristic self-organization in problems of engineering cybernetics, Automatica 6 (2) (1970) 207–219.
[35] C. Hebbi, H.R. Mamatha, Comprehensive dataset building and recognition of isolated handwritten kannada characters using machine learning models, Artificial Intelligence and Applicatons (2023). https://doi.org/10.47852/bonviewAIA3202624.
[36] Y. Guo, Z. Mustafaoglu, D. Koundal, Spam Detection Using Bidirectional Transformers and Machine Learning Classifier Algorithms, Journal of Computational and Cognitive Engineering (2022). https://doi.org/10.47852/bonviewJCCE2202192.
[37] B.K. Liu, W.Z. Lu, Surrogate models in machine learning for computational stochastic multi-scale modelling in composite materials design, Int. J. Hydromechatronics 5 (4) (2022) 336–365.
[38] H. Gaur, B. Khidhir, R.K. Manchiryal, Solution of structural mechanic's problems by machine learning, Int. J. Hydromechatronics 5 (1) (2022) 22–43.
[39] Z. Chen, Research on Internet Security Situation Awareness Prediction Technology based on Improved RBF Neural Network Algorithm, Journal of Computational and Cognitive Engineering (2022). https://doi.org/10.47852/bonviewJCCE149145205514.
[40] N. Luo, et al., Fuzzy logic and neural network-based risk assessment model for import and export enterprises: A review, Journal of Data Science and Intelligent Systems (2023). https://doi.org/10.47852/bonviewJDSIS32021078.
[41] B. Peng, et al., 3D-STCNN: Spatiotemporal Convolutional Neural Network based on EEG 3D features for detecting driving fatigue, Journal of Data Science and Intelligent Systems (2023). https://doi.org/10.47852/bonviewJDSIS3202983.
[42] L. Ma, et al., Apple grading method based on neural network with ordered partitions and evidential ensemble learning, CAAI Trans. Intell. Technol. 7 (4) (2022) 561–569. https://doi.org/10.1049/cit2.12140.
[43] P. Preethi, H.R. Mamatha, Region-based convolutional neural network for segmenting text in epigraphical images, Artificial Intelligence and Applicatons 1 (2) (2023) 119–127, https://doi.org/10.47852/bonviewAIA2202293.
[44] B. Yang, et al., Enhancing direct-path relative transfer function using deep neural network for robust sound source localization, CAAI Trans. Intell. Technol. 7 (3) (2022) 446–454. https://doi.org/10.1049/cit2.12024.
[45] B. Fan, et al., Intelligent vehicle lateral control based on radial basis function neural network sliding mode controller, CAAI Trans. Intell. Technol. 7 (3) (2022) 455–468. https://doi.org/10.1049/cit2.12075.
[46] S. Saminu, et al., Applications of artificial intelligence in automatic detection of epileptic seizures using EEG signals: A review, Artificial Intelligence and Applications 1 (1) (2023) 11–25. https://doi.org/10.47852/bonviewAIA2202297.
[47] A. Alizadeh, et al., Evaluation of the effects of the presence of ZnO -TiO_2 (50 %–50 %) on the thermal conductivity of Ethylene Glycol base fluid and its estimation using Artificial Neural Network for industrial and commercial applications, Journal of Saudi Chemical Society 27 (2) (2023) 101613. https://doi.org/10.1016/j.jscs.2023.101613.
[48] X. Dai, et al., Using Gaussian Process Regression (GPR) models with the Matérn covariance function to predict the dynamic viscosity and torque of SiO_2/Ethylene glycol nanofluid: A machine learning approach, Engineering Applications of Artificial Intelligence 122 (106107) (2023) 106107. https://doi.org/10.1016/j.engappai.2023.106107.